



Wind, Slick, and Fishing Boat Observations with Radarsat ScanSAR

Jim Gower and Simon Skey

The wide swath (450 km) of ScanSAR (synthetic aperture radar) images provides a greater opportunity for imaging surface phenomena and sporadic events, as well as fuller coverage of large-area patterns than the 100-km swaths of previous satellite SARs. To evaluate the ability of Radarsat ScanSAR to yield wind speed, we compare scaled radar intensities with wind speeds and directions measured by an array of buoys. The root-mean-square difference was less than 2 m/s in wind speed for 173 estimates. Among the Radarsat images were several showing large-scale dark slicks. Attempts to link these patterns to surfactants produced by bright plankton blooms detected in Advanced Very High Resolution Radiometer imagery were unsuccessful. Two images coincided with openings for seine fishing operations. In addition, boats with lengths of 18 to 25m were clearly visible, even though the radar signals were near the lower detection limit. (Keywords: Fishing boats, Plankton blooms, Radarsat ScanSAR, Wind speed.)

INTRODUCTION

This article presents three potential uses of Radarsat ScanSAR (synthetic aperture radar) imagery based on 24 ScanSAR-wide passes collected on the West Coast of Canada between April and August 1997 (Table 1). Examples are shown of the imaging of wind features, large-area slicks, and the relatively small boats used in coastal fishing. The area is well covered by an array of 16 meteorological buoys that transmit data hourly in real time. Buoy wind measurements are used to assess the potential of ScanSAR to yield quantitative wind data and to quantify the conditions under which radar images of other features are collected.

BACKGROUND

West Coast Meteorological Buoys

Figure 1 shows the locations of the 16 meteorological buoys that were deployed along and off the West Coast of Canada starting in 1987, with the final buoy in place by 1993. The three offshore buoys have the 4 × 6 m “Nomad” hulls; the near-shore buoys have a 3-m discus design. All buoys measure water and air temperature, wind speed and direction, waveheight and spectrum, and air pressure. In addition, buoy positions (latitude and longitude) are measured by the Global Positioning System (GPS) in case a buoy breaks loose

Date/time (UT, 1997)	Number of buoys	Wind speed (m/s)
9 April/1452	10	1.4–11.6
10 April/0216	11	6.9–12.2
13 April/0228	10	6.7–14.3
13 April/1437	5	5.4–10.3
20 April/0224	11	2.0–12.5
2 May/1521	4	7.2–15.3
3 May/0246	5	0.4–11.4
3 May/1453	9	4.5–9.4
16 May/1516	6	8.1–10.2
17 May/0239	8	6.5–9.4
17 May/1446	9	0.2–11.5
19 May/1528	2	10.9–15.4
27 May/1454	10	3.5–12.1
18 July/0229	10	3.3–11.6
25 July/0225	11	0.8–11.0
8 Aug/0217	11	1.4–12.5
11 Aug/0229	1	5.5–5.5
11 Aug/0230	8	5.1–11.6
11 Aug/1437	5	0.5–7.6
14 Aug/0243	5	8.0–11.8
14 Aug/1448	7	8.1–12.3
24 Aug/1457	10	6.5–14.4
25 Aug/1429	4	11.3–12.3
28 Aug/1442	1	5.3–5.3

from its mooring. All measurements are made at hourly intervals and are relayed in real time to users through the Geostationary Operational Environmental Satellite (GOES) and Anik satellite systems. The buoys are serviced annually or as soon as possible after being damaged by collision or storm. Buoy data are used routinely for weather forecasting, and the data time series are now becoming sufficiently long to use in climate studies of long-term trends. Buoy data have also been used to check the calibration of the European Remote Sensing (ERS-1) and Topex/Poseidon satellites. A program to install optical and other sensors on the buoys to collect data for comparison with the U.S. Sea-viewing Wide Field-of-View Sensor (SeaWiFS) and other water color satellites is now under way at the Canadian Institute of Ocean Sciences.

Radarsat ScanSAR Images

Radarsat ScanSAR images have a pixel separation of 50 m with a nominal resolution of 100 m. Images

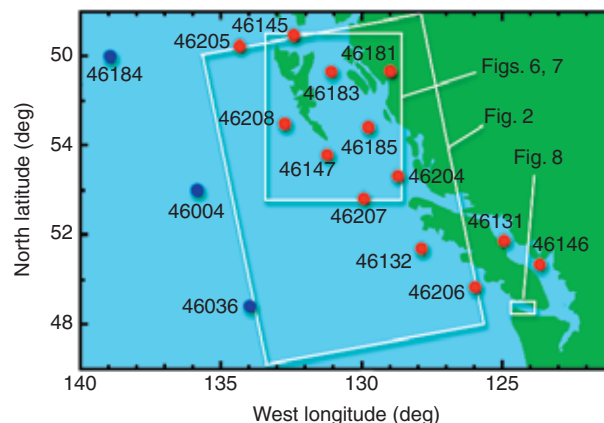


Figure 1. Map showing code numbers and locations of the 16 West Coast meteorological buoys operated by Environment Canada and the Department of Fisheries and Oceans. Red circles represent 3-m discus buoys; blue circles are larger, offshore “Nomad” buoys. Areas covered by other figures in this article are also shown.

have about 10,000 lines each of 10,000 8-bit single-byte pixels, although some passes were provided for this work in continuous swaths up to 30,000 lines long. Data were initially received on Exabyte tape and transcribed to CD for ease of handling. To reduce the speckle and image volume, software was written at the Institute of Ocean Sciences to average the images to a pixel separation of 500×500 m (10×10 box-car averaging). This appeared to preserve all the wind- and slick-related spatial structure present in the images.

Most of the passes imaged in this study (Table 1) were selected for high winds, although some of the later passes were selected for calm conditions that were expected to make slick patterns visible. The passes imaged an average of seven buoys each.

An example of one of the more interesting images, taken at 13 April 1997 at 0228 UT (18:28 PST on 12 April), is shown in Fig. 2. Figure 2a shows the averaged image with the strong signal gradient present from the near edge (left) to the far edge (right). Figure 2b shows the same image “flattened,” that is, adjusted to remove this variation with pixel number. After flattening, the recomputed image value r_f from the raw average bit count value r is

$$r_f = r/[0.25 + (p/1200)^3],$$

where p is the pixel number. Since all images count p from the far-range edge, this formula can be applied to both ascending and descending passes. The number of pixels per line varies from about 960 to 1120, but the average parameters used in this formula were found adequate for all cases. They were applied only to improve the display of the data, and not in the buoy/Radarsat comparison discussed in the next section.

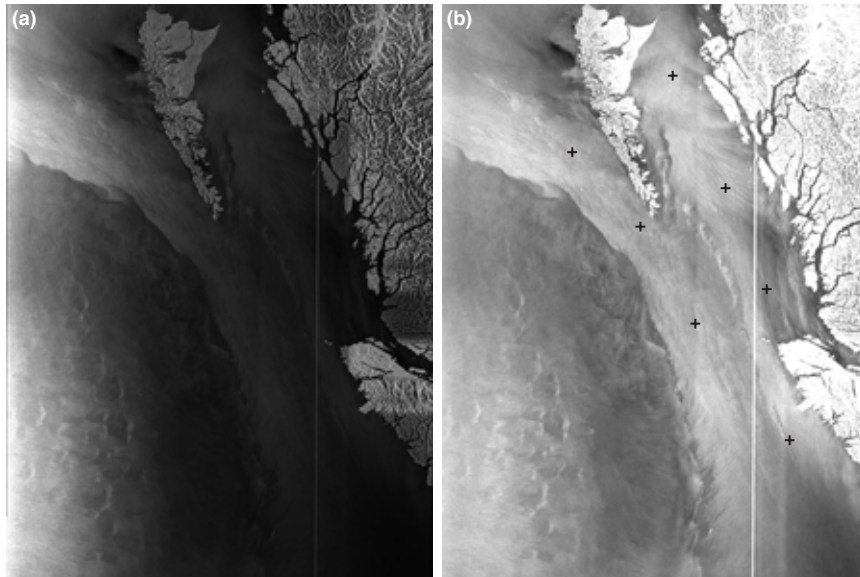


Figure 2. Radarsat ScanSAR image from 13 April 1997 at 0228 UT (local dusk on 12 April): (a) raw image and (b) image corrected by the multiplicative factors given in the text. Positions of seven meteorological buoys are indicated by crosses. Swath width (horizontal) is 450 km. (© Canadian Space Agency, 1997.)

Most ScanSAR images show a very visible, narrow, vertical line, variable in brightness and slightly variable in range position. This is a known problem due to a nadir ambiguity in one of the image swaths used in making up the ScanSAR coverage. Fainter systematic variations of signal with range are also common over the ocean, as in Fig. 2b, indicating poor calibration of the images.

In Fig. 2b, a large-scale wind pattern consisting of an arc of strong wind (high radar return, buoy measurements up to 14 m/s) is clearly visible. To the west of this arc, lower winds show a patchy structure that appears to indicate gusts associated with downdrafts. Crosses indicate the positions of buoys at which wind measurements were made. Wind along the coast was from the southeast. Streaks in the along-wind direction near buoys suggest that wind direction could be determined using fast Fourier transforms of subareas of the image.

OBSERVATIONS

Winds

Software was written to extract average signal levels from the averaged SAR images at the nominal locations of the buoys. GPS measurements were used to confirm the accuracy of the nominal positions. Actual buoy positions can vary by an amount comparable to the water depth, which for the offshore Nomad buoys is about 3.4 km. For the buoys in open water near the coast, depths range from 2.0 to 2.9 km, with the exception of the southernmost buoy (46206, Fig. 1), which is on La Perouse Bank in 73 m of water. All other buoys in protected waters are in depths of less than

300 m. GPS measurements confirm this variation in position, showing root-mean-square (rms) variations in latitude and longitude equal to about half of the water depths. Position errors will therefore be significant for this study when wind speed varies over a scale of a few kilometers. Time errors may also play a part where winds are variable in time. Buoy measurements are averaged over 10 min and are recorded once per hour. Time differences of up to 30 min are therefore present in the comparisons.

The 24 Radarsat swaths available for this study correspond to 173 sets of synchronous ground truth measurements (wind speed and direction) from the buoys (Table 1). We use these measurements to calculate

radar scattering cross sections (σ_0) using the CMOD-IFR2 algorithm, which is an improved version of CMOD4. These models are derived for vertical (VV) polarization, but cross-sectional differences between the VV and the horizontal (HH) polarization of Radarsat (up to a few decibels) are expected to vary slowly with radar incidence angle at the target pixel. Also, Radarsat is calibrated so that R_0 values are equivalent to β_0 , the signal power per unit range element, rather than the σ_0 derived by the model, which is the signal power per unit surface area of ocean. The conversion $\sigma_0 = \beta_0 \sin(\theta)$ also introduces a variation with incidence angle θ .

We convert Radarsat signal (raw 8-bit count) values r to power measurements R in decibels using

$$R = 10 \log_{10}(r^2/k),$$

where k is a constant. This relation assumes that pixel values r are proportional to signal voltage and are squared to measure power. In the absence of quantitative calibration information for this Radarsat ScanSAR imagery, k is chosen to bring the R values into closest agreement with the model output. The best fit using this relation for R shows a slope of 0.81 Radarsat decibel per buoy decibel. To add incidence-angle dependence—as expected from the differences between HH and VV polarizations—and σ_0 and β_0 , the expression is changed to

$$R = 10 \log_{10}[r^2/(k \sin^n \theta)].$$

It was found that n could be adjusted to bring the two results (Radarsat, buoy) into good agreement.

Figure 3 shows the result for $k = 68,600$ and $n = 1$. Points represented in red are those for which the measured wind speed was 1.5 m/s or less. Of these 10 points, 3 show significant deviation from the mean relation. One would expect low radar returns to be more strongly affected by calibration errors that result in signal offsets. Alternatively, higher spatial variability under calm conditions may be causing additional scatter. Excluding the low wind points, the scatter about the mean line is 1.39 dB rms for a total of 165 points, with $r^2 = 0.94$.

We have allowed two free parameters in fitting R to the model output: the constant (k) and the power (n) to which $\sin(\theta)$ is raised. This assumes that the polarization difference is a function only of θ and not of wind speed or relative direction, and can be approximated by such a power. The conversion from σ_0 to β_0 requires an exponent of $\sin(\theta)$ equal to -1.0 . We find that a value near 1.0 gives the best fit, both in the slope of the mean relation (ideally = 1) and in the scatter of points (r^2 value). For example, a value $n = -1.0$ gives a slope of 0.66 and $r^2 = 0.89$; $n = 0$ gives a slope of 0.81 and $r^2 = 0.94$; $n = 1.0$ gives a slope of 0.96 and $r^2 = 0.94$. An "optimum" occurs for an exponent n of 1.25 when slope = 1.0 and $r^2 = 0.94$. The optimum value of n is also expected to show minimum systematic variation with the incidence angle of the Radarsat/buoy difference in decibels or in derived wind speed (Fig. 5).

A large part of the correlation shown in Fig. 3 is due to the strong dependence of signal level on incidence angle evident in Fig. 2a and in all (unflattened) Radarsat imagery. Higher returns are observed from lower incidence angles, as predicted by the models.

Figure 4 shows the comparison presented in terms of wind speed. To make this comparison, the wind direction values measured by the buoys are used in the CMOD-IFR2 model, and the input wind speed is adjusted until the model output agrees with the σ_0 derived from the Radarsat imagery. This procedure allows for the complex directional properties of the model, which prevent a direct calculation of wind speed.

The contribution of the incidence angle to the correlation is now removed, so that the points are more scattered than in Fig. 3. Low wind speed points are plotted, but most correspond to low predicted and measured winds and fall in the lower left corner of the plot. Two points (upper left) represent high Radarsat winds in measured calm conditions. These are the two points that lie significantly above the mean relation in Fig. 3. One of these occurred in a coastal area with strong variation of backscatter near the buoy site, the other just after passage of a strong wind front.

Omitting these two outlying points, the mean relation shows a slope of 0.98, with an average wind speed

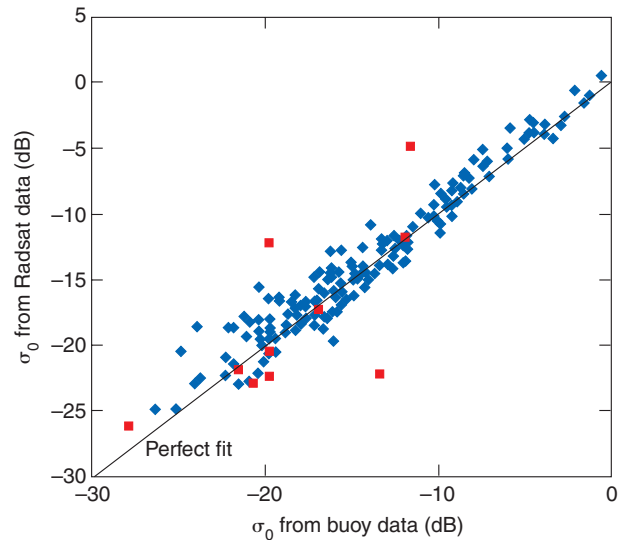


Figure 3. Predicted and observed radar returns. The line of perfect agreement is shown. Red squares correspond to a measured wind speed of 1.5 m/s or less.

offset of 1.0 m/s. The best-fit line with zero intercept has a slope of 1.09. The rms value of the difference between buoy and Radarsat wind speeds is 1.94 m/s ($r^2 = 0.70$, 171 points), or 1.72 m/s about the best-fit line with zero intercept. A plot of this error against incidence angle (Fig. 5) shows that the points at low incidence angle give slightly higher scatter. If low ($<26^\circ$) incidence angle (near-range) points are removed, the wind speed error = 1.63 m/s rms for 148

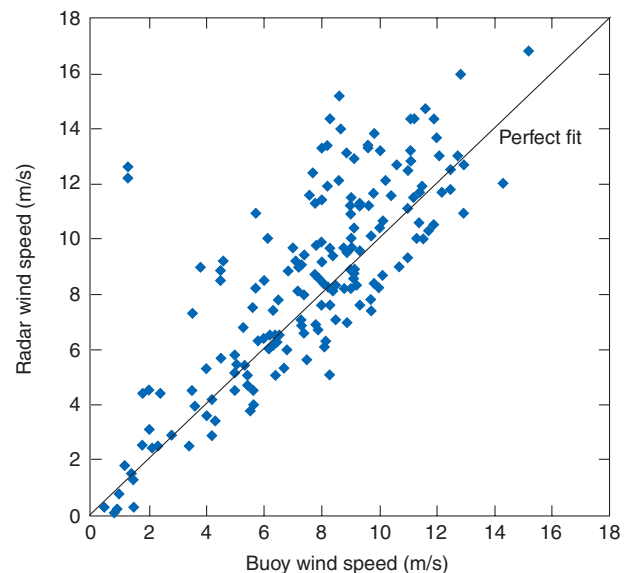


Figure 4. Wind speeds calculated from Radarsat data at buoy locations compared with measurements made by the buoys. Wind directions measured by the buoys are used in the calculation of Radarsat winds. Two of the three outlying points in Fig. 3 can be seen in this plot; the third (below the line) is near the origin.

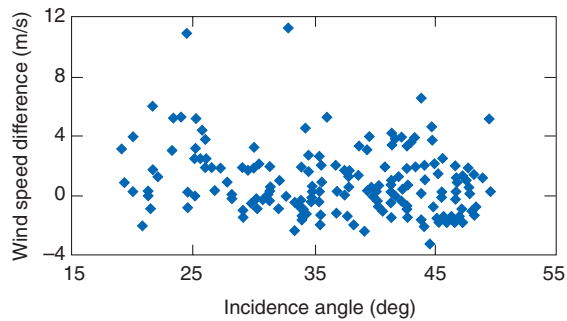


Figure 5. Difference between Radarsat and buoy wind speeds plotted against incidence angle. The two outlying points shown in Fig. 4 can be seen here also. No systematic variation of wind speed difference with incidence angle is evident.

points. If, in addition, high ($>40^\circ$) incidence angle (far-range) points are removed, the wind speed error = 1.44 m/s rms for 78 points.

No evidence was found in this analysis for a Radarsat “noise floor,” or for a digitization offset from zero, either of which would imply that a zero pixel value would correspond to non-zero radar backscatter power. This would introduce errors at low signals and far range, which are not apparent in Figs. 3 or 5. Other translations that use look-up tables to fit the image values into an 8-bit range are possible, but our results confirm our assumption that the pixel values r are proportional to signal voltage.

Slicks

Large, spatially complex dark areas have been noted in the SAR imagery of coastal waters in many parts of the world, and are identified with calm conditions and the naturally occurring surfactants derived from a combination of terrigenous and marine productivity. The patterns have been mapped on the coast of British Columbia using ERS-1 imagery, but the ScanSAR mode of Radarsat provides the wider swath needed to cover the continental shelf and nearby waters, and hence to delineate the full extent of the slick-affected areas.

We observed several examples of slick patterns on the coast and can demonstrate the link to low wind conditions using data from the array of meteorological buoys (Fig. 1). Some of the surfactants that cause the slicks may be by-products of primary productivity (phytoplankton growth) on the shelf. This would indicate an important link between radar observations and marine biology. Others are of terrigenous origin, being derived from organic material washed from the land in freshwater runoff. Slick patterns and their motions can also provide information on surface currents.

Radarsat showed major slick patterns on only four of the swaths listed in Table 1. Two appeared on 11 and 28 August off the southwest coast of Vancouver Island,

and two were observed on 25 July and 8 August east of the Queen Charlotte Islands in Hecate Strait. For the latter two patterns, buoy 46183 showed wind speeds of 1.0 and 1.6 m/s respectively, from the west. The second of these two images shows a calm slick area east of the islands (Fig. 6).

Figure 7 shows part of a time sequence of images derived from Advanced Very High Resolution Radiometer (AVHRR) satellite imagery for Hecate Strait, east of the Queen Charlotte Islands, during August 1997. Water brightened by suspended material (inorganic sediment, or plankton blooms) is shown using the “gain-weighted” difference between signals from bands 1 and 2 of the AVHRR instrument. The weight is adjusted to optimize suppression of cloud and Sun-glint signals.^{1,2} “Bright water” is first clearly visible on 8 August as parallel streams that appear to originate off the islands near the mainland coast. By 13 August, this bright water is concentrated in the center of the strait, and has dispersed by about 23 August. Such a long-term bright water event, occurring in relatively calm conditions, indicates a major plankton bloom.

The 25 July image showed slicks in this area before the start of the satellite image sequence. The 8 August Radarsat image (Fig. 6) coincides with the clear image in the top left panel of Fig. 7. The patterns show no obvious similarity to Fig. 6. The radar image shows a stronger wind blowing in Dixon Entrance, north of the Queen Charlottes, and buoy 46145 confirms this with a measurement of 7.5 m/s from a heading of 300° . This wind blows across the northeast corner of the Queen Charlottes and obscures any slick pattern in Fig. 6 north of buoy 46183 in the brightest area of the bloom shown in Fig. 7. Slick patterns in radar images will also be affected by local variations in atmospheric boundary-layer stability caused by differences between air and sea surface temperature. Buoy measurements of sea and air temperatures do not suggest that this is significant here.

The slick in Fig. 6 may be due to surfactants from phytoplankton growth, and it is suggestive that a plankton bloom was detected in AVHRR imagery in this area at the same time. However, the AVHRR imagery detected no earlier event that would have provided the surfactants needed to make the slicks in Fig. 6. The SeaWiFS imager now provides greatly improved images of phytoplankton distribution and may confirm a link with slicks imaged by radar.

Fishing Boats

On 11 and 25 August 1997, three openings occurred in the tightly controlled British Columbian seine fishery for salmon. The salmon are netted as they return to their spawning grounds, passing either to the south of Vancouver Island through Juan de Fuca Strait

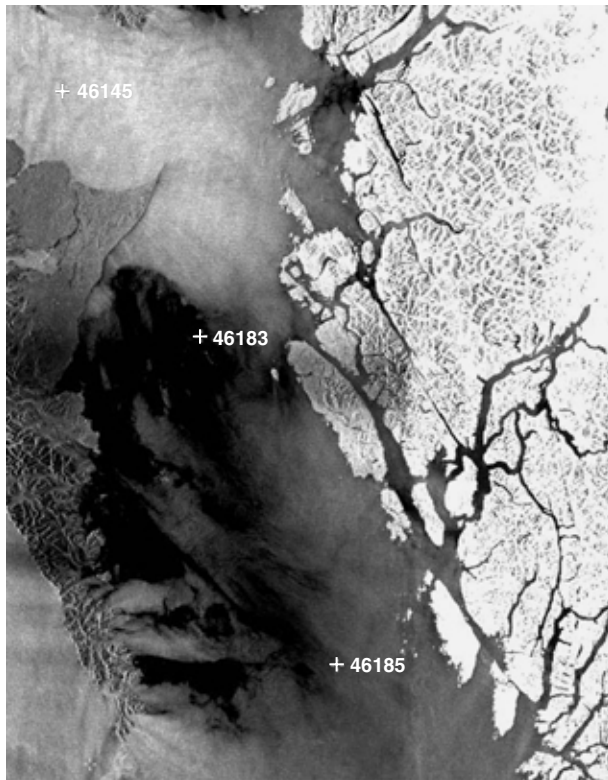


Figure 6. Radarsat image taken on 8 August 1997 at 0217 UT (local dusk on 7 August), showing calm and slick areas east of the Queen Charlotte Islands at the time of the bloom event illustrated in Fig. 7. Locations of three weather buoys (Fig. 1) are shown.

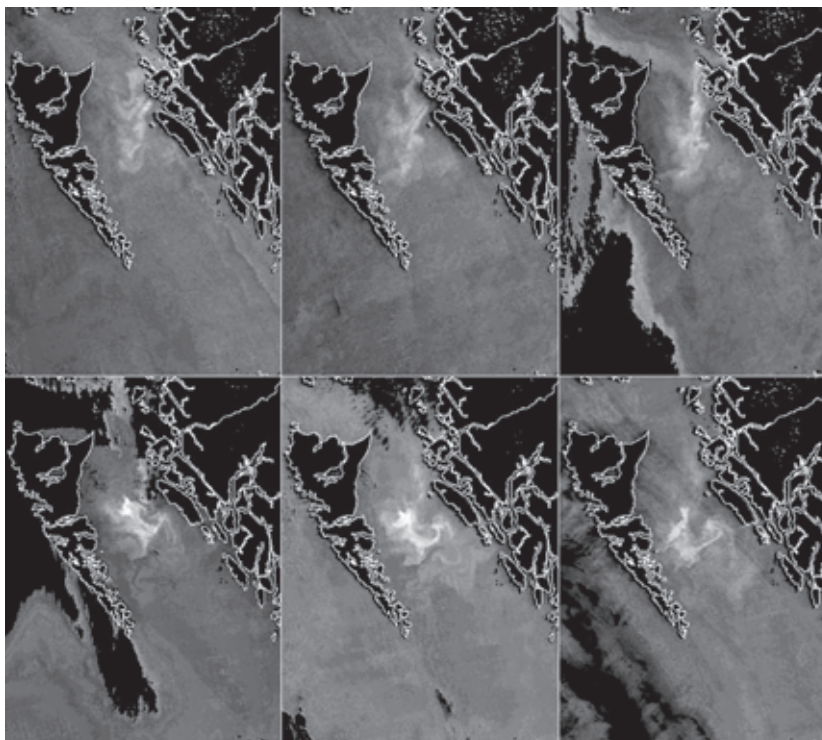


Figure 7. Part of a daily sequence of rectified AVHRR images showing water brightened by plankton blooms in Hecate Strait, east of the Queen Charlotte Islands, in August 1997. Cloud and land are masked to black. A coastline is added in white. Top row, 8–10 August; bottom row, 13–15 August. The event was visible on most days from 5–20 August.

or to the north of the island through Johnstone Strait. In the early 1900s, the southern route was the more important, but in the past 20 years a significant diversion has occurred, making Johnstone Strait the main route today. There is some indication that increased diversion occurs in “El Niño” years. The percentage of diversion continues to be hotly discussed, especially as its prediction is crucial to managing the fishery.

Figure 8 shows a small portion of a Radarsat ScanSAR image taken on 25 August 1997 at 1429 UT (07:29 PDT) covering the western (entrance) end of Juan de Fuca Strait. The start of a 2-day seine fishery opening occurred at 1400 UT (07:00 PDT), so the image shows the boats making their first sets, i.e., net deployments. These boats are estimated to be to 18 to 25 m long (mostly the latter), and are therefore point targets on ScanSAR imagery, which has a nominal resolution of 100 m. Radar backscatter will vary with boat orientation, shape, and material and can sometimes give strong returns.

According to Hop Wo et al.,³ “The seine fishery in Area 20 is referred to as a ‘Blue Line’ fishery. This consists of vessels operating along fishing lines perpendicular to the shore, with fishing location dependent on ocean depth and operating distance between fishing vessels.” The “Blue Line” (oceanward boundary of permissible fishing) is near the left edge of Fig. 8. According to records of the Canadian Department of

Fisheries and Oceans, 55 boats took part in this 2-day opening. In Fig. 8, 43 boats are located in the pattern of short lines extending southward from the north shore of the strait.

To quantify detection, we have fitted point-target return shapes to the image at locations where a pixel value exceeded a given threshold. The returns were assumed to be circularly symmetrical and with a Gaussian, i.e., $\exp(-r^2/a)$, profile having variable width a . Figure 8 shows the result of marking the positions of 53 of these targets that fulfill width, signal strength, and signal-to-background ratio criteria. It can be seen that, in addition to 43 returns in the pattern of seine boats, 10 other point targets were detected from other areas. Although two of these returns are probably genuine, the others suggest that the chosen criteria are starting to allow “false alarms.”

In this example, Radarsat successfully imaged the pattern of

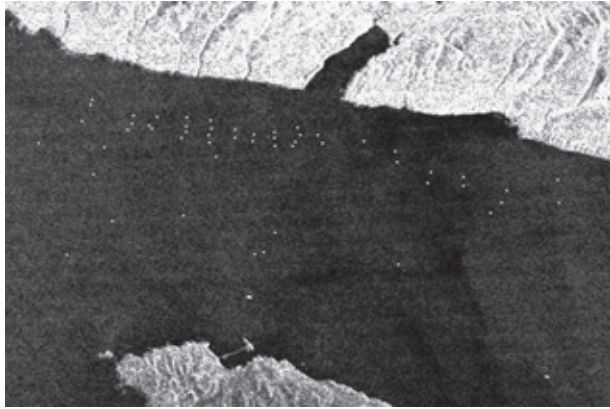


Figure 8. Seine fishing boats imaged on 25 August 1997 at 1429 UT (07:29 PDT) during a 36-h opening starting at 1400 UT (07:00 PDT). The positions of the targets are identified on the basis of signal strength, signal-to-background ratio, and point-like width. (© Canadian Space Agency, 1997.)

boats, detecting about 80% of expected targets even at this small size range. Higher-resolution modes of Radarsat are clearly required for better boat detection, but their reduced swath widths make coverage of openings that occur in limited areas for limited times increasingly rare as resolution increases and swath width narrows. Figure 8 appears to demonstrate a role for satellite radar in the monitoring of fishing efforts around the world.

SUMMARY

Several conclusions can be derived from this study.

- Artifacts such as those visible in Fig. 2 indicate that these ScanSAR images, provided by the Canadian Data Processing Facility, are not fully calibrated. Therefore, although these images are a major new satellite product, at present unique to Radarsat, they cannot be fully exploited. We understand that progress is being made to address this problem.
- Progress is also being made in producing a standard model for predicting HH-polarized radar returns at C band, comparable to the VV models used here (personal communication, Vachon of CCRS and Dobson of the Bedford Oceanographic Institute, June 1999; see also the article by Thompson and Beal, this issue). The present buoy data set should contribute to this effort when the Radarsat imagery is calibrated.

- Radarsat ScanSAR images clearly show wind patterns over almost their entire swath, with a moderate amount of quantitative information. The study reported here was based on a small sample of images. An expanded study is needed to cover a fuller range of high wind conditions and show the wide variety of wind-related features (e.g., fronts, downdraft cells, and topographic effects of interest to meteorologists and oceanographers).
- Insufficient examples of slicks were obtained to fulfill the goal of demonstrating a link with plankton blooms, or of making use of the movement of the slicks to measure surface currents. Blooms were observed using AVHRR images (Fig. 7) at the same time and in the same area as slicks were observed by Radarsat (Fig. 6), but the link to surfactants from coastal primary productivity, although suggestive, is inconclusive.
- The wide swath of ScanSAR resulted in coverage of 3 seine fishery openings in Johnstone and Juan de Fuca Straits, out of the 23 that occurred in the period from July to October 1997. Other openings may have been covered by other images not available to this project. The changing requirements of fisheries management make openings hard to predict, and the large areas that need to be covered make the wide ScanSAR swath width an essential attribute for this as for most other types of ship detection.

REFERENCES

- ¹Gower, J. F. R., "Red Tide Monitoring Using AVHRR HRPT Imagery from a Local Receiver," *Remote Sens. Environ.* **48**, 309–318 (1994).
- ²Gower, J. F. R., "Bright Plankton Blooms on the West Coast of North America Observed with AVHRR Imagery," Chap. 2, in *Monitoring Algal Blooms: New Techniques for Detecting Large Scale Environmental Change*, Kahru and Brown (eds.), Landes Bioscience, Austen, TX, pp. 25–41 (1997).
- ³Hop Wo, L., Ryall, P. J., and Lewis, D. M., *Area 20 Commercial Salmon Fishery By-Catch Monitoring Program, 1994 and 1995*, Can. Manusc. Rep. Fish. Aquat. Sci. 2166 (1997).

THE AUTHORS

JIM GOWER is with the Institute of Ocean Sciences, Sidney, BC, Canada. His e-mail address is gowerj@df0-mpo.gc.ca.

SIMON SKEY is with Axy's Environmental Consulting Ltd., Sidney, BC, Canada. His e-mail address is skey@axys.com.